INTERNATIONAL JOURNAL OF
NUMERICAL ANALYSIS AND MODELING
Volume 18, Number 3, Pages 324–338

ERROR ESTIMATES FOR THE LAPLACE INTERPOLATION ON CONVEX POLYGONS

WEIWEI ZHANG, LONG HU, ZONGZE YANG, AND YUFENG NIE

Abstract. In the natural element method (NEM), the Laplace interpolation error estimate on convex planar polygons is proved in this study. The proof is based on bounding gradients of the Laplace interpolation for convex polygons which satisfy certain geometric requirements, and has been divided into several parts that each part is bounded by a constant. Under the given geometric assumptions, the optimal convergence estimate is obtained. This work provides the mathematical analysis theory of the NEM. Some numerical examples are selected to verify our theoretical result.

Key words. Natural element method, geometric constraints, Laplace interpolation, error estimate.

1. Introduction

In engineering practice, many problems in mechanics and physics can be reduced to solve mathematical problems of ordinary differential equations or partial differential equations under given boundary conditions. With the rapid development of computer technology, many numerical methods such as weighted residual method, finite element method, finite difference method, meshless method [1] and boundary element method have been developed to solve the engineering problems.

In recent decades, meshless methods have emerged, such as smooth particle hydrodymics method (SPH) [2, 3], reproducing kernel particle method (RKPM) [4], moving least-square approximation method (MLS) [5], the partition of unity method [6], radial basis functions (RBF) [7], point interpolation method (PIM) [8] and natural element method (NEM) [9], and these methods have been developed to solve partial differential equations (PDEs). In the meshless method, shape functions are constructed in terms of a group of discrete nodes, and no predefined nodal connectivity is required. The nodes are unstructured and can be freely moved, inserted and deleted. The meshless method does not need to generate mesh, thus it has some advantages in handling crack propagation or large deformation problems.

The NEM is a meshless method based on the concept of natural neighbor interpolants and on the discretization by Voronoi diagram and Delaunay triangulation. The NEM interpolant is constructed on the basis of Voronoi diagram [10], which is unique for a given set of distinct nodes in the plane. It means that the NEM interpolant is determined once the location of nodes is determined. The dual Delaunay triangles [11] are constructed for nodal integration and numerical computation of the interpolant. However, unlike finite element method (FEM) where angle restrictions are imposed on the triangles for the convergence of the method, there are no such constraints on the size, shape, and angles of the triangles in NEM. Unlike most of meshless methods, the natural neighbor interpolants have the properties of interpolation of nodal data, allowing direct imposition of essential boundary conditions as FEM does. On the other hand, the NEM presents some characteristics of meshless methods, such as accurate shape functions with quasi-spherical influence

Received by the editors November 1, 2020.
2000 *Mathematics Subject Classification.* 65N30, 65N50.

zones and robust approximations with no user-defined parameter on non-uniform grids, and it can handle complex geometry or crack propagation problems easily. In general, the NEM not only has the advantages of finite element method and meshless method, but also overcomes some of their shortcomings.

Since Braun and Sambridge [9] firstly introduced NEM in 1995, many researchers have applied it to solve mechanical problems. Sukumar et al. [12, 13] used NEM to study the application of elliptic boundary value problems for elastic mechanics, and constructed the C^1 natural neighbor interpolation to solve fourth-order elliptic partial differential equations. Cueto et al. [14, 15] used α-shapes in the context of NEM to ensure the linear precision of the interpolant over convex and non-convex boundaries. Bueche et al. [16] investigated NEM in two-dimensional linear elastodynamics and studied vibration and wave propagation problem. Toi Yutaka [17, 18] analyzed the elastic-plastic problem and brittle fracture problem with NEM. Cai and Zhu [19, 20] used a local Petrov-Galerkin method to establish a global equilibrium equation, which has fast convergence rate and high accuracy. Gonzalez [21] established a novel algorithm to simulate free-surface fluid dynamics phenomena. Alfaro [22] used NEM to simulate hollow profiles. Cho et al. [23] presented a mixed natural element approximation of Reissner-Mindlin plate for the locking-free numerical analysis of plate-like thin elastic structures.

The application of NEM has been developed for about twenty years [24, 25], while the theoretical research of convergence, stability and error analysis is rare and needs to be studied deeply. Gillette et al. [26] made a brief study on the error estimates for generalized barycentric interpolation, including the Sibson interpolation. Alexander et al. [27] proved interpolation error estimates for the mean value coordinates over convex polygons. In a similar fashion to estimates shown for different coordinates in these papers, we study another interpolation error of NEM-Laplace interpolation.

The rest of the paper is organized as follows. In Section 2, we review the relevant background on geometric constraints, Laplace interpolation and interpolation theory in Sobolev Spaces. In Section 3, the estimate is divided into several parts and the initial estimate is established for each part. Our result is obtained in Theorem 2 which gives a constant bound on the gradients of the Laplace interpolation. In Section 4, two numerical examples are given to verify our analysis. Finally the conclusion is drawn in Section 5.

2. Background

2.1. Geometric constraints. Let Ω be a convex polygon in $\mathbb{R}^2$, which consists of n nodes, $\boldsymbol{x}_1, \boldsymbol{x}_2, \cdots, \boldsymbol{x}_n$, and let the interior angle at $\boldsymbol{x}_i$ be β_i. The largest distance between two points in Ω is denoted by $diam(\Omega)$ and the radius of the largest inscribed circle is denoted $\rho(\Omega)$, then the aspect ratio γ is defined as $\gamma := \frac{diam(\Omega)}{\rho(\Omega)}$. Now we give the following geometric constraints.

G1. Bounded aspect ratio: There exists a constant $\gamma^* > 0$ such that $2 \leq \gamma \leq \gamma^*$.

G2. Minimum edge length: There exists a constant $d^* > 0$ such that $|\boldsymbol{x}_i - \boldsymbol{x}_j| \geq d^*$ for all $i \neq j$.

G3. Maximum interior angle: There exists a constant $\beta^* > 0$ such that $\beta_i < \beta^* < \pi$ for all i.

Under the above geometric constraints, two other closely related properties also hold.

G4. Minimum interior angle: There exists a constant $\beta_* > 0$ such that $\beta_i > \beta_* > 0$ for all i.

G5. Maximum vertex count: There exists a constant $n^* > 0$ such that $n \leq n^*$.
In [26], it is shown that G1 $\Rightarrow$ G4, G2 $\Rightarrow$ G5 and G3 $\Rightarrow$ G5.

2.2. Laplace interpolation. The Laplace interpolation is based on the construction of the Voronoi diagram and Delaunay tessellation. Suppose a set of distinct nodes $S = \{\boldsymbol{x}_1, \boldsymbol{x}_2, ..., \boldsymbol{x}_n\}$ in $\mathbb{R}^2$. In mathematical terms, the Voronoi cell $V(\boldsymbol{x}_i)$ is defined as

$$V(\boldsymbol{x}_i) = \{\boldsymbol{x} \in \mathbb{R}^2 | d(\boldsymbol{x}, \boldsymbol{x}_i) < d(\boldsymbol{x}, \boldsymbol{x}_j), \forall j \neq i\}, \tag{1}$$

where $d(\boldsymbol{x}, \boldsymbol{x}_i)$ is the distance between $\boldsymbol{x}$ and $\boldsymbol{x}_i$ in Euclidean metric, see Figure 1(a). The Delaunay triangulation (DT), which is the straight-line dual of the Voronoi diagram, is constructed by connecting the nodes whose Voronoi cells have common boundaries, see Figure 1(b). If a point $\boldsymbol{x}$ lies within the circumcircle of triangle $DT(\boldsymbol{x}_i, \boldsymbol{x}_j, \boldsymbol{x}_k)$, then $\boldsymbol{x}_i$, $\boldsymbol{x}_j$ and $\boldsymbol{x}_k$ are called the natural neighbor nodes of $\boldsymbol{x}$. See Figure 1(c), $\boldsymbol{x}$ lies within the circumcircle of triangle $DT(1, 2, 3)$ and $DT(1, 3, 4)$, then 1, 2, 3 and 4 are the natural neighbor nodes of $\boldsymbol{x}$.

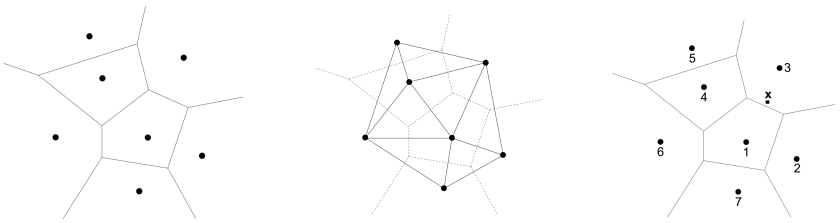

(a) Voronoi cell (b) Delaunay triangulation (c) natural neighbor nodes of $\boldsymbol{x}$

FIGURE 1. Geometric structures.

Having found all natural neighbor nodes of $\boldsymbol{x}$, the new Voronoi cell related to $\boldsymbol{x}$ can be constructed by its natural neighbor nodes which can be seen in Figure 2(a), where Q_i $(i = 1, 2, \cdots, 4)$ denote the vertices of the Voronoi edges, then the Laplace interpolation can be determined as follows. Suppose the number of the natural neighbor nodes is M, then Voronoi cell of $\boldsymbol{x}$ have M sides. Denote the lengths of the Voronoi edges by s_i, $i = 1, 2, \cdots, M$. Denote further the lengths of the altitudes drawn from $\boldsymbol{x}$ to ith sides by h_i, $i = 1, 2, \cdots, M$, see Figure 2(b). Then the Laplace interpolation of $\boldsymbol{x}$ is defined as

$$\phi_i(\boldsymbol{x}) = \frac{\lambda_i(\boldsymbol{x})}{\sum_{j=1}^{M} \lambda_j(\boldsymbol{x})}, \tag{2}$$

where

$$\lambda_i(\boldsymbol{x}) = \frac{s_i(\boldsymbol{x})}{h_i(\boldsymbol{x})}. \tag{3}$$

Consider another representation of Laplace interpolation. Suppose $\boldsymbol{x}_{i-1}$, $\boldsymbol{x}_i$, $\boldsymbol{x}_{i+1}$ are some natural neighbor nodes of $\boldsymbol{x}$ (sorted counterclockwise). Let Q_1 and Q_2 denote two vertices of the Voronoi edges, $\varphi_1 = \angle Q_1 \boldsymbol{x} \boldsymbol{x}_i$ and $\varphi_2 = \angle Q_2 \boldsymbol{x} \boldsymbol{x}_i$, see

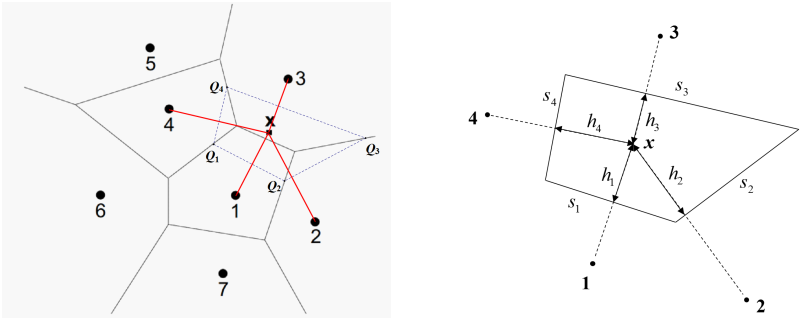

(a) New Voronoi cell related to $\boldsymbol{x}$ (b) the Laplace interpolation of $\boldsymbol{x}$

FIGURE 2. The Voronoi cell and Laplace interpolation of $\boldsymbol{x}$.

Figure 3. According to the definition of Laplace interpolation, (3) can be rewritten as

$$\lambda_i(\boldsymbol{x}) = \frac{|Q_1Q_2|}{\frac{|\boldsymbol{x}\boldsymbol{x}_i|}{2}} = \frac{\frac{|\boldsymbol{x}\boldsymbol{x}_i|}{2}\tan\varphi_1 + \frac{|\boldsymbol{x}\boldsymbol{x}_i|}{2}\tan\varphi_2}{\frac{|\boldsymbol{x}\boldsymbol{x}_i|}{2}} = \tan\varphi_1 + \tan\varphi_2. \tag{4}$$

In $\Delta\boldsymbol{x}\boldsymbol{x}_i\boldsymbol{x}_{i-1}$, it is easy to get that

$$2\angle\varphi_1 + 2\angle\boldsymbol{x}\boldsymbol{x}_{i-1}Q_1 + 2\angle Q_1\boldsymbol{x}_{i-1}\boldsymbol{x}_i = \pi, \tag{5}$$

then

$$\varphi_1 = \frac{\pi}{2} - \angle\boldsymbol{x}\boldsymbol{x}_{i-1}\boldsymbol{x}_i, \tag{6}$$

and

$$\varphi_2 = \frac{\pi}{2} - \angle\boldsymbol{x}\boldsymbol{x}_{i+1}\boldsymbol{x}_i. \tag{7}$$

Hence substituting (6) and (7) into (4), we can obtain that

$$\lambda_i(\boldsymbol{x}) = \cot\angle\boldsymbol{x}\boldsymbol{x}_{i-1}\boldsymbol{x}_i + \cot\angle\boldsymbol{x}\boldsymbol{x}_{i+1}\boldsymbol{x}_i. \tag{8}$$

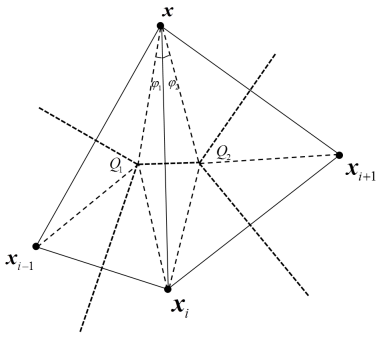

FIGURE 3. Some of natural neighbor nodes of $\boldsymbol{x}$.

The interpolate approximation $u^h(\boldsymbol{x})$ in the discrete solution space can be expressed as

$$u^h(\boldsymbol{x}) = \sum_{i=1}^{n} \phi_i(\boldsymbol{x})u_i \tag{9}$$

where u_i is the discrete solution at node x_i.

The natural neighbor interpolation has some remarkable properties which are listed in the following[12]

- **Non-negativity:**

$$0 \leq \phi_i(\boldsymbol{x}) \leq 1. \tag{10}$$

- **Interpolation:**

$$\phi_i(\boldsymbol{x}_j) = \delta_{ij}. \tag{11}$$

- **Partition of unity:**

$$\sum_{i=1}^{n} \phi_i(\boldsymbol{x}) = 1. \tag{12}$$

- **Linear Completeness:**

$$\boldsymbol{x} = \sum_{i=1}^{n} \phi_i(\boldsymbol{x})\boldsymbol{x}_i. \tag{13}$$

- **Smoothness:** The Laplace interpolation shape function is C^∞ at any point except at nodal locations as well as on the boundary of the Delaunay circles, where they are C^0.

2.3. Interpolation in Sobolev Spaces. Interpolation error estimates are typically derived from the Bramble-Hilbert lemma and its improvements. The modern version of the Bramble-Hilbert lemma is stated below.

Lemma 1 (see [28])**.** *Let $\Omega \subset R^{n'}$ be a bounded convex domain. For all $u(\boldsymbol{x}) \in W_p^m(\Omega)$, where $W_p^m(\Omega)$ is the Sobolev space, $m \in \mathbb{N}$, $1 \leq p \leq \infty$, there exists a polynomial $P(\boldsymbol{x})$ of total degree $m-1$ for which*

$$\|u(\boldsymbol{x}) - P(\boldsymbol{x})\|_{k,p} \leq C(n', m)(diam(\Omega))^{m-k}\|u(\boldsymbol{x})\|_{m,p}, \quad k = 0, 1, \cdots, m \tag{14}$$

where $C(n', m)$ is a constant depending on n' and m only.

According to Lemma 1 and above geometric constraints, we have the following theorem for natural neighbor interpolation.

Theorem 1. *Let Ω be a bounded convex domain which consists of n nodes, set $diam(\Omega) = 1$ and the domain satisfies G1 and G5. The interpolation operator $Iu(x)$ is defined as $Iu(\boldsymbol{x}) = \sum_{i=1}^{n} \phi_i(\boldsymbol{x})u(\boldsymbol{x}_i)$, where $\phi_i(\boldsymbol{x})$ is the natural neighbor interpolation of node i. If there exists a constant C_ϕ such that*

$$\|\phi_i\|_{H^k(\Omega)} \leq C_\phi, \quad k = 0, 1 \tag{15}$$

then for all $u(\boldsymbol{x}) \in W_p^m(\Omega)$,

$$\|u - Iu\|_{H^k(\Omega)} \leq C\|u\|_{H^2(\Omega)}, \quad k = 0, 1 \tag{16}$$

where C is a constant depending on n^* and C_ϕ.

Proof. As mentioned above, the natural neighbor interpolation has the property of linear completeness, see (13). Then $IP(\boldsymbol{x}) = P(\boldsymbol{x})$ for any first order polynomial

$P(\boldsymbol{x})$, which yields the estimate

$$\begin{aligned}
\|u-Iu\|_{H^k(\Omega)} &\le \|u-P\|_{H^k(\Omega)} + \|P-Iu\|_{H^k(\Omega)} \\
&= \|u-P\|_{H^k(\Omega)} + \|I(P-u)\|_{H^k(\Omega)} \\
&\le \|u-P\|_{H^k(\Omega)} + \sum_{i=1}^{n} |P(\boldsymbol{x}_i)-u(\boldsymbol{x}_i)| \cdot \|\phi_i\|_{H^k(\Omega)} \\
&\le \|u-P\|_{H^k(\Omega)} + n^* C_\phi \|P-u\|_{C^0(\overline{\Omega})} \qquad (17) \\
&\le \|u-P\|_{H^2(\Omega)} + n^* C_\phi C_S \|P-u\|_{H^2(\Omega)} \\
&\le (1+n^* C_\phi C_S)\|u-P\|_{H^2(\Omega)} \\
&\le (1+n^* C_\phi C_S) C(2,2)\|u\|_{H^2(\Omega)} \\
&= C\|u\|_{H^2(\Omega)}
\end{aligned}$$

where C_S is the Sobolev embedding, i.e., $\|u\|_{C^0(\overline{\Omega})} \le C_S\|u\|_{H^2(\Omega)}$. □

Corollary 1. *Let $diam(\Omega) \le 1$. If the conditions of Theorem 1 hold, then for all $u(\boldsymbol{x}) \in W_p^m(\Omega)$,*

$$\|u-Iu\|_{H^k(\Omega)} \le C diam(\Omega)^{2-k}\|u\|_{H^2(\Omega)}, \quad k=0,1. \tag{18}$$

Theorem 1 and its corollary imply that the Laplace interpolation error estimate can be demonstrated if (15) holds, and our next work is to prove it.

3. Laplace interpolation error estimate

The domain of influence of the shape function $\phi_i(\boldsymbol{x})$ demonstrates that the value of $\phi_i(\boldsymbol{x})$ will increases radially when $\boldsymbol{x} \to \boldsymbol{x}_i$. For simplicity, assume that $diam(\Omega) = 1$ and $\boldsymbol{x} \in B(\boldsymbol{x}_i, \frac{d^*}{\gamma^*})$, where $B(\boldsymbol{x}_i, \frac{d^*}{\gamma^*})$ denotes a circle with node $\boldsymbol{x}_i$ as its center and $\frac{d^*}{\gamma^*}$ as its radius. According to (2) and (8), the Laplace interpolation can be rewritten as

$$\phi_i(\boldsymbol{x}) = \frac{\lambda_i(\boldsymbol{x})}{\sum_{j=1}^{M}\lambda_j(\boldsymbol{x})} = \frac{\cot\angle\boldsymbol{x}\boldsymbol{x}_{i-1}\boldsymbol{x}_i + \cot\angle\boldsymbol{x}\boldsymbol{x}_{i+1}\boldsymbol{x}_i}{\sum_{j=1}^{M}(\cot\angle\boldsymbol{x}\boldsymbol{x}_{j-1}\boldsymbol{x}_j + \cot\angle\boldsymbol{x}\boldsymbol{x}_{j+1}\boldsymbol{x}_j)}. \tag{19}$$

Let $t_{i-1,i} := \cot\angle\boldsymbol{x}\boldsymbol{x}_{i-1}\boldsymbol{x}_i$, then the gradient of $\phi_i(\boldsymbol{x})$ can be expressed as

(20)

$$\begin{aligned}
\nabla\phi_i(\boldsymbol{x}) &= \frac{\nabla\lambda_i(\boldsymbol{x})\sum_{j=1}^{M}\lambda_j(\boldsymbol{x}) - \lambda_i(\boldsymbol{x})\sum_{j=1}^{M}\nabla\lambda_j(\boldsymbol{x})}{(\sum_{j=1}^{M}\lambda_j(\boldsymbol{x}))^2} \\
&= \frac{\nabla(t_{i-1,i}+t_{i+1,i})\sum_{j=1}^{M}(t_{j-1,j}+t_{j+1,j}) - (t_{i-1,i}+t_{i+1,i})\sum_{j=1}^{M}\nabla(t_{j-1,j}+t_{j+1,j})}{(\sum_{j=1}^{M}(t_{j-1,j}+t_{j+1,j}))^2}.
\end{aligned}$$

Now we present the estimate of (20), which can be divided into several parts. Each part is bounded by a constant, as shown in Lemma 2, Lemma 3 and Lemma 4.

Lemma 2. *Under conditions G1 and G2, there is a constant C_1 such that*

$$|\nabla t_{i-1,i}t_{i,i-1} - t_{i-1,i}\nabla t_{i,i-1}| \le C_1(\sum_{j=1}^{M}(t_{j-1,j}+t_{j+1,j}))^2 \tag{21}$$

for all $i = 1, 2, \cdots, n$.

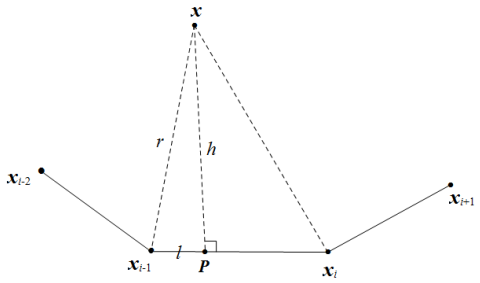

FIGURE 4. Some of natural neighbor nodes of $\boldsymbol{x}$ for Lemma 2.

Proof. As shown in Figure 4, the segment $\boldsymbol{xP}$ is perpendicular to the given segment $\boldsymbol{x}_{i-1}\boldsymbol{x}_i$. Defining $d = |\boldsymbol{x}_i\boldsymbol{x}_{i-1}|$, $h = |\boldsymbol{xP}|$, $l = |\boldsymbol{x}_{i-1}\boldsymbol{P}|$, $r = |\boldsymbol{x}_{i-1}\boldsymbol{x}|$. Without loss of generality, let $\boldsymbol{x}_{i-1} = (0,0)$, $\boldsymbol{x}_i = (x_i, ky_i)$ and $\boldsymbol{x} = (x,y)$, $k < \infty$, then we find that

$$t_{i-1,i} = \frac{l}{h} = \left|\frac{x+ky}{kx-y}\right|, \tag{22}$$

$$t_{i,i-1} = \frac{d-l}{h} = \frac{d\sqrt{1+k^2}}{|kx-y|} - \left|\frac{x+ky}{kx-y}\right|. \tag{23}$$

As a result,

$$|\nabla t_{i-1,i}t_{i,i-1} - t_{i-1,i}\nabla t_{i,i-1}| = \frac{(k^2+1)d}{(kx-y)^2} = \frac{d}{h^2} = \frac{d}{l^2}t_{i-1,i}^2. \tag{24}$$

(24) also holds when $k{=}\infty$.

Since $\boldsymbol{x} \in B(\boldsymbol{x}_i, \frac{d^*}{\gamma^*}) \subset B(\boldsymbol{x}_i, \frac{d^*}{2})$ and $d \geq d^*$, it follows that $l \geq d - \frac{d^*}{2} \geq \frac{d^*}{2}$, and $d \leq diam(\Omega) = 1$, thus

$$|\nabla t_{i-1,i}t_{i,i-1} - t_{i-1,i}\nabla t_{i,i-1}| \leq \frac{4d}{d^{*2}}t_{i-1,i}^2 \leq \frac{4}{d^{*2}}\Big(\sum_{j=1}^{M}(t_{j-1,j} + t_{j+1,j})\Big)^2 \tag{25}$$

which completes the proof. □

Lemma 3. *Under conditions G1,G2 and G3, there is a constant C_2 such that*

$$|\nabla t_{i-1,i}t_{i,i+1} - t_{i-1,i}\nabla t_{i,i+1}| \leq C_2\Big(\sum_{j=1}^{M}(t_{j-1,j} + t_{j+1,j})\Big)^2 \tag{26}$$

for all $i = 1, 2, \cdots, n$.

Proof. According to the triangle inequality,

$$|\nabla t_{i-1,i}t_{i,i+1} - t_{i-1,i}\nabla t_{i,i+1}| \leq |\nabla t_{i-1,i}t_{i,i+1}| + |t_{i-1,i}\nabla t_{i,i+1}| \tag{27}$$

holds, then our goal is to give the estimates of the above two absolute values. As shown in Figure 5, the segment $\boldsymbol{xP}'$ is perpendicular to the given segment $\boldsymbol{x}_i\boldsymbol{x}_{i+1}$, defining $d' = |\boldsymbol{x}_i\boldsymbol{x}_{i+1}|$, $h' = \left|\boldsymbol{xP}'\right|$, $l' = \left|\boldsymbol{x}_{i+1}\boldsymbol{P}'\right|$ and $r' = |\boldsymbol{x}_{i+1}\boldsymbol{x}|$. Let $\boldsymbol{x}_{i-1} = (0,0)$, $\boldsymbol{x}_i = (x_i, ky_i)$ and $\boldsymbol{x} = (x,y)$. According to the value of $\angle\boldsymbol{x}\boldsymbol{x}_i\boldsymbol{x}_{i+1}$, two cases is considered in the following.

***Case* 1**: $\frac{1}{2}\angle\boldsymbol{x}_{i-1}\boldsymbol{x}_i\boldsymbol{x}_{i+1} \leq \angle\boldsymbol{x}\boldsymbol{x}_i\boldsymbol{x}_{i+1} \leq \angle\boldsymbol{x}_{i-1}\boldsymbol{x}_i\boldsymbol{x}_{i+1}$.

In this case, $h \leq h'$, as shown in Figure 5(a). By (22), we have

$$|\nabla t_{i-1,i}| = \left|\nabla\frac{x+ky}{kx-y}\right| = \frac{r}{h^2}, \tag{28}$$

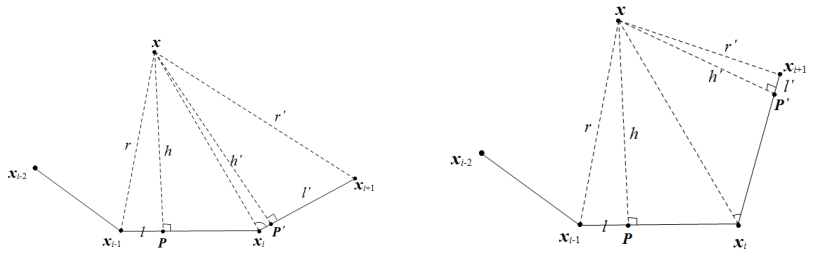

FIGURE 5. Some of natural neighbor nodes of $\boldsymbol{x}$ for Lemma 3. (a) *Case* 1, (b) *Case* 2.

and

$$|t_{i,i+1}| = |\cot \angle \boldsymbol{x}\boldsymbol{x}_i\boldsymbol{x}_{i+1}| \le \max\{\left|\cot \frac{1}{2}\angle \boldsymbol{x}_{i-1}\boldsymbol{x}_i\boldsymbol{x}_{i+1}\right|, |\cot \angle \boldsymbol{x}_{i-1}\boldsymbol{x}_i\boldsymbol{x}_{i+1}|\}. \tag{29}$$

Similarly, it is easy to get that

$$\begin{aligned} |\nabla t_{i,i+1}| &= \frac{|\boldsymbol{x}\boldsymbol{x}_i|}{h'^2} = \frac{1}{h' \sin \angle \boldsymbol{x}\boldsymbol{x}_i\boldsymbol{x}_{i+1}} \\ &\le \frac{1}{h \min\{\left|\sin \frac{1}{2}\angle \boldsymbol{x}_{i-1}\boldsymbol{x}_i\boldsymbol{x}_{i+1}\right|, |\sin \angle \boldsymbol{x}_{i-1}\boldsymbol{x}_i\boldsymbol{x}_{i+1}|\}}. \end{aligned} \tag{30}$$

According to (22), (28) and (29), we have

(31)

$$\begin{aligned} |\nabla t_{i-1,i}t_{i,i+1}| &\le \frac{r \cdot \max\{\left|\cot \frac{1}{2}\angle \boldsymbol{x}_{i-1}\boldsymbol{x}_i\boldsymbol{x}_{i+1}\right|, |\cot \angle \boldsymbol{x}_{i-1}\boldsymbol{x}_i\boldsymbol{x}_{i+1}|\}}{l^2} t_{i-1,i}^2 \\ &\le \frac{\max\{\left|\cot \frac{1}{2}\angle \boldsymbol{x}_{i-1}\boldsymbol{x}_i\boldsymbol{x}_{i+1}\right|, |\cot \angle \boldsymbol{x}_{i-1}\boldsymbol{x}_i\boldsymbol{x}_{i+1}|\}}{\left(\frac{d^*}{2}\right)^2} \left(\sum_{j=1}^{M} (t_{j-1,j} + t_{j+1,j})\right)^2 \\ &\le \frac{4\max\{\left|\cot \frac{\beta_*}{2}\right|, |\cot \beta^*|\}}{d^{*2}} \left(\sum_{j=1}^{M} (t_{j-1,j} + t_{j+1,j})\right)^2. \end{aligned}$$

According to (22) and (30), we have

$$\begin{aligned} |t_{i-1,i}\nabla t_{i,i+1}| &\le \frac{l}{h^2 \min\{\left|\sin \frac{1}{2}\angle \boldsymbol{x}_{i-1}\boldsymbol{x}_i\boldsymbol{x}_{i+1}\right|, |\sin \angle \boldsymbol{x}_{i-1}\boldsymbol{x}_i\boldsymbol{x}_{i+1}|\}} \\ &= \frac{1}{l \min\{\left|\sin \frac{1}{2}\angle \boldsymbol{x}_{i-1}\boldsymbol{x}_i\boldsymbol{x}_{i+1}\right|, |\sin \angle \boldsymbol{x}_{i-1}\boldsymbol{x}_i\boldsymbol{x}_{i+1}|\}} t_{i-1,i}^2 \\ &\le \frac{2}{d^* \min\{\left|\sin \frac{\beta_*}{2}\right|, |\sin \beta^*|\}} \left(\sum_{j=1}^{M} (t_{j-1,j} + t_{j+1,j})\right)^2. \end{aligned} \tag{32}$$

Collecting (31) and (32), the result of Lemma 3 can be proved.

***Case* 2**: $0 \le \angle \boldsymbol{x}\boldsymbol{x}_i\boldsymbol{x}_{i+1} \le \frac{1}{2}\angle \boldsymbol{x}_{i-1}\boldsymbol{x}_i\boldsymbol{x}_{i+1}$.

In this case, $h' \le h$. As shown in Figure 5(b), $t_{i,i+1} = \frac{d'-l'}{h'}$. If $0 \le \angle \boldsymbol{x}_{i-1}\boldsymbol{x}_i\boldsymbol{x}_{i+1} < \frac{\pi}{2}$, then

$$(d' - l') \sin \frac{\angle \boldsymbol{x}_{i-1}\boldsymbol{x}_i\boldsymbol{x}_{i+1}}{2} \le (d' - l') \tan \frac{\angle \boldsymbol{x}_{i-1}\boldsymbol{x}_i\boldsymbol{x}_{i+1}}{2} \le h;$$

else if $\frac{\pi}{2} \le \angle \boldsymbol{x}_{i-1}\boldsymbol{x}_i\boldsymbol{x}_{i+1} < \pi$, then

$$(d' - l') \sin \angle \boldsymbol{x}_{i-1}\boldsymbol{x}_i\boldsymbol{x}_{i+1} \le h.$$

Hence,

$$d^{'} - l^{'} \leq \max\{\frac{h}{\sin\frac{\angle \boldsymbol{x}_{i-1}\boldsymbol{x}_i\boldsymbol{x}_{i+1}}{2}}, \frac{h}{\sin\angle \boldsymbol{x}_{i-1}\boldsymbol{x}_i\boldsymbol{x}_{i+1}}\} \leq \max\{\frac{h}{\sin\frac{\beta_*}{2}}, \frac{h}{\sin\beta^*}\}. \tag{33}$$

Then we have

$$\begin{aligned} |\nabla t_{i-1,i}t_{i,i+1}| &= \frac{r}{h^2}\cdot\frac{d^{'}-l^{'}}{h^{'}} \leq \frac{1}{h^{'2}}\max\{\frac{1}{\sin\frac{\beta_*}{2}}, \frac{1}{\sin\beta^*}\} \\ &= \frac{1}{l^{'2}}\max\{\frac{1}{\sin\frac{\beta_*}{2}}, \frac{1}{\sin\beta^*}\}\cdot t_{i+1,i}^2 \\ &\leq \frac{4}{d^{*2}}\max\{\frac{1}{\sin\frac{\beta_*}{2}}, \frac{1}{\sin\beta^*}\}\cdot(\sum_{j=1}^{M}(t_{j-1,j}+t_{j+1,j}))^2. \end{aligned} \tag{34}$$

From Figure 5(b),

$$\frac{h}{|\boldsymbol{x}\boldsymbol{x}_i|} = \sin\angle\boldsymbol{x}\boldsymbol{x}_i\boldsymbol{x}_{i-1} \geq \min\{\left|\sin\frac{1}{2}\angle\boldsymbol{x}_{i-1}\boldsymbol{x}_i\boldsymbol{x}_{i+1}\right|, |\sin\angle\boldsymbol{x}_{i-1}\boldsymbol{x}_i\boldsymbol{x}_{i+1}|\}.$$

As a result, we can obtain that

$$\begin{aligned} |t_{i-1,i}\nabla t_{i,i+1}| &= \frac{l}{h}\cdot\frac{|\boldsymbol{x}\boldsymbol{x}_i|}{h^{'2}} \leq \frac{l}{h^{'2}\min\{\left|\sin\frac{1}{2}\angle\boldsymbol{x}_{i-1}\boldsymbol{x}_i\boldsymbol{x}_{i+1}\right|, |\sin\angle\boldsymbol{x}_{i-1}\boldsymbol{x}_i\boldsymbol{x}_{i+1}|\}} \\ &= \frac{l}{l^{'2}\min\{\left|\sin\frac{1}{2}\angle\boldsymbol{x}_{i-1}\boldsymbol{x}_i\boldsymbol{x}_{i+1}\right|, |\sin\angle\boldsymbol{x}_{i-1}\boldsymbol{x}_i\boldsymbol{x}_{i+1}|\}}\cdot t_{i+1,i}^2 \\ &\leq \frac{4}{d^{*2}\min\{\left|\sin\frac{\beta_*}{2}\right|, |\sin\beta^*|\}}\cdot(\sum_{j=1}^{M}(t_{j-1,j}+t_{j+1,j}))^2. \end{aligned} \tag{35}$$

Putting (34) and (35) together gives the result.

In each case, the desired estimate holds. Taking the maximum constant over each case completes the proof. □

Lemma 4. *Under conditions G1,G2 and G3, there is a constant C_3 such that*

$$|\nabla t_{i-1,i}t_{m-1,m} - t_{i-1,i}\nabla t_{m-1,m}| \leq C_3(\sum_{j=1}^{M}(t_{j-1,j}+t_{j+1,j}))^2, \quad \forall m \neq i, i+1 \tag{36}$$

$$|\nabla t_{i-1,i}t_{m,m-1} - t_{i-1,i}\nabla t_{m,m-1}| \leq C_3(\sum_{j=1}^{M}(t_{j-1,j}+t_{j+1,j}))^2, \quad \forall m \neq i, i+1 \tag{37}$$

for all $i = 1, 2, \cdots, n$.

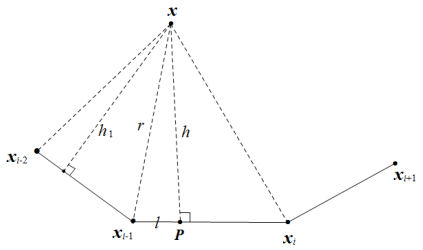

FIGURE 6. Some of natural neighbor nodes of $\boldsymbol{x}$ for Lemma 4.

Proof. According to the triangle inequality,

$$|\nabla t_{i-1,i}t_{m,m-1} - t_{i-1,i}\nabla t_{m,m-1}| \le |\nabla t_{i-1,i}t_{m,m-1}| + |t_{i-1,i}\nabla t_{m,m-1}| \tag{38}$$

holds, and our goal is to give the estimates of the above two absolute values. Without loss of generality, consider one of these cases, $\nabla t_{i-1,i}t_{i-1,i-2} - t_{i-1,i}\nabla t_{i-1,i-2}$. Denote the distance from node $\boldsymbol{x}$ to the line segment $\boldsymbol{x}_{i-1}\boldsymbol{x}_{i-2}$ by h_1, as shown in Figure 6. Since $\boldsymbol{x} \in B(\boldsymbol{x}_i, \frac{d^*}{\gamma^*})$, we have

$$\angle \boldsymbol{x}_i\boldsymbol{x}_{i-1}\boldsymbol{x}_{i-2} - \arcsin\frac{d^*}{d\gamma^*} \le \angle \boldsymbol{x}\boldsymbol{x}_{i-1}\boldsymbol{x}_{i-2} \le \angle \boldsymbol{x}_i\boldsymbol{x}_{i-1}\boldsymbol{x}_{i-2},$$

then

$$\begin{aligned} t_{i-1,i-2} &= \cot \angle \boldsymbol{x}\boldsymbol{x}_{i-1}\boldsymbol{x}_{i-2} \\ &\le \max\{\left|\cot(\angle \boldsymbol{x}_i\boldsymbol{x}_{i-1}\boldsymbol{x}_{i-2} - \arcsin\frac{d^*}{d\gamma^*})\right|, |\cot \angle \boldsymbol{x}_i\boldsymbol{x}_{i-1}\boldsymbol{x}_{i-2}|\} \\ &\le \max\{\left|\cot(\beta_* - \arcsin\frac{1}{\gamma^*})\right|, |\cot \beta^*|\}, \end{aligned} \tag{39}$$

and

$$\begin{aligned} \frac{h_1}{r} &= \sin \angle \boldsymbol{x}\boldsymbol{x}_{i-1}\boldsymbol{x}_{i-2} \\ &\ge \min\{\left|\sin(\angle \boldsymbol{x}_i\boldsymbol{x}_{i-1}\boldsymbol{x}_{i-2} - \arcsin\frac{d^*}{d\gamma^*})\right|, |\sin \angle \boldsymbol{x}_i\boldsymbol{x}_{i-1}\boldsymbol{x}_{i-2}|\} \\ &\ge \min\{\left|\sin(\beta_* - \arcsin\frac{1}{\gamma^*})\right|, |\sin \beta^*|\}. \end{aligned} \tag{40}$$

According to (28) and (39), we have

$$\begin{aligned} |\nabla t_{i-1,i}t_{i-1,i-2}| &\le \frac{r}{h^2}\max\{\left|\cot(\beta_* - \arcsin\frac{1}{\gamma^*})\right|, |\cot \beta^*|\} \\ &\le \frac{1}{l^2}\max\{\left|\cot(\beta_* - \arcsin\frac{1}{\gamma^*})\right|, |\cot \beta^*|\} \cdot t_{i-1,i}^2 \\ &\le \frac{4\max\{\left|\cot(\beta_* - \arcsin\frac{1}{\gamma^*})\right|, |\cot \beta^*|\}}{{d^*}^2}(\sum_{j=1}^{M}(t_{j-1,j} + t_{j+1,j}))^2, \end{aligned} \tag{41}$$

and

$$\begin{aligned} |t_{i-1,i}\nabla t_{i-1,i-2}| &= \frac{l}{h}\cdot\frac{r}{h_1^2} \\ &\le \frac{l}{h^2\min\{\left|\sin(\beta_* - \arcsin\frac{1}{\gamma^*})\right|, |\sin \beta^*|\}} \\ &= \frac{1}{l\min\{\left|\sin(\beta_* - \arcsin\frac{1}{\gamma^*})\right|, |\sin \beta^*|\}} \cdot t_{i-1,i}^2 \\ &\le \frac{2}{d^*\min\{\left|\sin(\beta_* - \arcsin\frac{1}{\gamma^*})\right|, |\sin \beta^*|\}}(\sum_{j=1}^{M}(t_{j-1,j} + t_{j+1,j}))^2. \end{aligned} \tag{42}$$

Collecting (41) and (42) completes the proof. □

Now we give the following theorem.

Theorem 2. *Under conditions G1,G2 and G3, there is a constant C such that*

$$\|\phi_i\|_{H^k(\Omega)} \le C, \quad k = 0, 1 \tag{43}$$

for all $i = 1, 2, \cdots, n$.

Proof. By (10), we have

$$\|\phi_i\|_{L^2(\Omega)} \leq (meas(\Omega))^{\frac{1}{2}} \leq \frac{\sqrt{\pi}}{2}. \tag{44}$$

To obtain the estimate of $|\nabla\phi_i(x)|$, we partition the summands of the numerator according to similar terms in Lemma 2, Lemma 3 and Lemma 4, and thus get the following result

(45)

$$\begin{aligned}
|\nabla\phi_i(\boldsymbol{x})| &= \left| \frac{\nabla\lambda_i(\boldsymbol{x}) \sum_{j=1}^{M} \lambda_j(\boldsymbol{x}) - \lambda_i(\boldsymbol{x}) \sum_{j=1}^{M} \nabla\lambda_j(\boldsymbol{x})}{(\sum_{j=1}^{M} \lambda_j(\boldsymbol{x}))^2} \right| \\
&= \left| \frac{\nabla(t_{i-1,i} + t_{i+1,i}) \sum_{j=1}^{M} (t_{j-1,j} + t_{j+1,j}) - (t_{i-1,i} + t_{i+1,i}) \sum_{j=1}^{M} \nabla(t_{j-1,j} + t_{j+1,j})}{(\sum_{j=1}^{M} (t_{j-1,j} + t_{j+1,j}))^2} \right| \\
&\leq 2C_1 + 2C_2 + (4n^* - 8)C_3.
\end{aligned}$$

Putting these together, we have

$$\begin{aligned}
\|\phi_i\|_{H^1(\Omega)} &\leq \|\phi_i\|_{L^2(\Omega)} + |\phi_i|_{H^1(\Omega)} \\
&\leq (1 + 2C_1 + 2C_2 + (4n^* - 8)C_3)(meas(\Omega))^{\frac{1}{2}} \\
&\leq (1 + 2C_1 + 2C_2 + (4n^* - 8)C_3) \cdot \frac{\sqrt{\pi}}{2} \\
&= C,
\end{aligned} \tag{46}$$

which is the desired upper bound. Thus, Theorem 2 guarantees that the optimal interpolation error estimate (16) holds. □

4. Numerical Results

In this section, two numerical examples are given to verify the computed convergence rate is very close to the theoretical optimal rate in NEM, which show the correctness of the theoretical results of this paper.

4.1. Example 1. In the first example, we consider the following Poisson equation

$$-\Delta u = 8\pi^2 \cos 2\pi x \sin 2\pi y$$

in a square domain $\Omega = [0, 1]^2$ with a circular hole centered at (0.5, 0.5), and the radius of the circle is defined as 0.2. The Dirichlet boundary conditions are suitably defined such that the exact solution is

$$u = \cos 2\pi x \sin 2\pi y.$$

The nodal discretization and valid Delaunay triangulation are shown in Figure 7. Using the

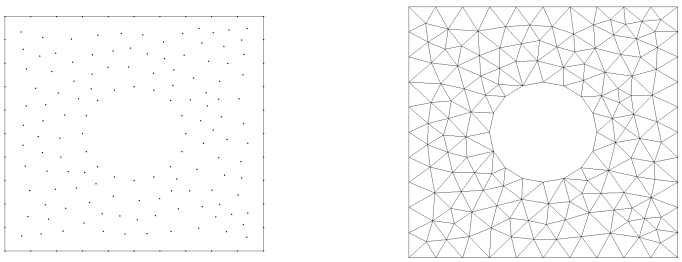

FIGURE 7. Node distribution and corresponding Delaunay triangulation.

TABLE 1. The L^2 norm and H^1 norm of the relative errors and convergence rate for Example 1.

$\#nodes$	$Mesh\ size$	$\frac{\|u-u^h\|_{L^2}}{\|u\|_{L^2}}$	R_L	$\frac{\|u-u^h\|_{H^1}}{\|u\|_{H^1}}$	R_H
98	0.12	5.6815e-2	–	19.7149e-2	–
344	0.06	1.4145e-2	2.0060	10.0749e-2	0.9685
1280	0.03	0.3854e-2	1.8759	5.2103e-2	0.9513
4928	0.015	0.1045e-2	1.8829	2.7048e-2	0.9458

NEM, the L^2 norm and H^1 norm of the relative errors and the corresponding convergence rates (R_L and R_H) are given in Table 1. From Table 1 we can see that the convergence orders in the two norms are 2 and 1 respectively, which verifies our theoretical analysis.

Figure 8 shows the comparison of the relative errors in the L^2 norm and the H^1 norm using the FEM and NEM respectively, where the numbers with brackets represent the values of ordinate. It is observed that although the same convergence rates are obtained for the two methods, the numerical results of the NEM have higher precision than that of the FEM.

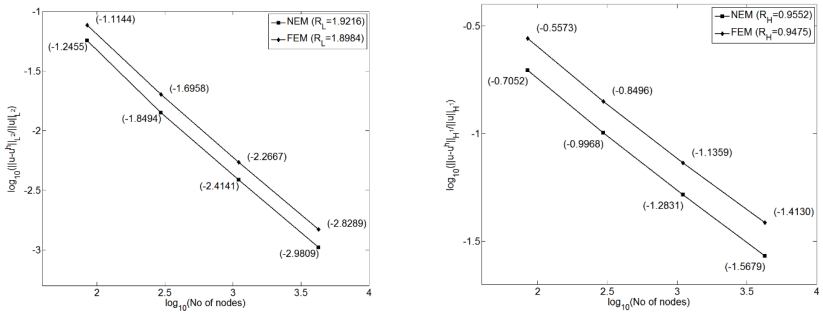

(a) (b)

FIGURE 8. Convergence rate for Example 1. (a) L^2 norm, (b) H^1 norm.

4.2. Example 2. Consider the cantilever beam shown in Figure 9, which has a vertical upward force $P = -1000$N at the end. The beam has characteristic length $L = 4$m, height $D = 1$m and unit thickness, and it is assumed to be in a state of plane stress without considering the gravity. The elasticity modulus $E = 3 \times 10^5$Pa, and Poisson's ratio $\gamma = 0.25$. The displacement vector solution is given by

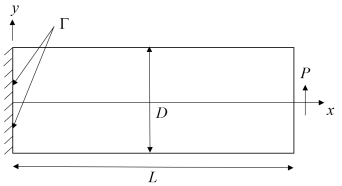

FIGURE 9. Cantilever beam.

TABLE 2. Relative error norms and convergence rate for Example 2.

$\#nodes$	$\frac{\|\boldsymbol{u}-\boldsymbol{u}^h\|}{\|\boldsymbol{u}\|}$	R	$\frac{\|\boldsymbol{u}-\boldsymbol{u}^h\|_E}{\|\boldsymbol{u}\|_E}$	R_E
85	6.6553e-2	–	18.7149e-2	–
297	1.6322e-2	2.0277	9.6560e-2	1.1434
1105	0.4057e-2	2.0083	4.9620e-2	1.0458
4257	0.1013e-2	2.0018	2.0217e-2	1.0073

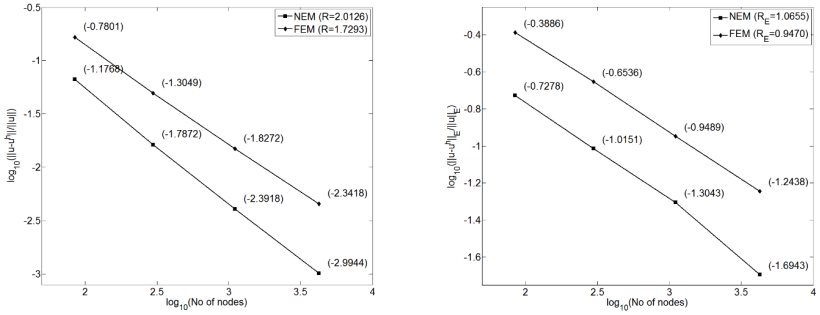

(a) (b)

FIGURE 10. Convergence rate for Example 2. (a) Displacement, (b) energy.

$$
\begin{aligned}
u(x,y) &= \frac{-Py}{6EI}\left[(6L-3x)\,x+(2+\gamma)\,y^2-\frac{3D^2}{2}\,(1+\gamma)\right],\\
v(x,y) &= \frac{P}{6EI}\left[3\gamma y^2\,(L-x)+(3L-x)\,x^2\right],
\end{aligned}
\tag{47}
$$

while the stresses are

$$
\begin{aligned}
\sigma_{xx} &= \frac{-P\,(L-x)\,y}{I},\\
\sigma_{yy} &= 0,\\
\sigma_{xy} &= \frac{P}{2I}\left(\frac{D^2}{4}-y^2\right),
\end{aligned}
\tag{48}
$$

where $I{=}\frac{D^3}{12}$ is the moment of inertia for a beam with rectangular cross-section and unit thickness.

The problems are carried out using three different regular nodal discretizations, namely 85(17*5) nodes, 297(33*9) nodes and 1105(65*17) nodes. The displacement and energy norms are defined as

$$
\begin{aligned}
\|\boldsymbol{u}\| &= \Big(\int_\Omega (u^2+v^2)d\Omega\Big)^{\frac{1}{2}},\\
\|\boldsymbol{u}\|_E &= \Big(\frac{1}{2}\int_\Omega (\varepsilon-\varepsilon^h)^T C(\varepsilon-\varepsilon^h)d\Omega\Big)^{\frac{1}{2}},
\end{aligned}
\tag{49}
$$

where C is the elasticity matrix. The displacement and energy relative error norms and the convergence rates (R and R_E) are given in Table 2 and Figure 10(The numbers with brackets represent the values of ordinate in Figure 10).

According to the results in Table 2, the convergence rate for the cantilever beam is close to the theoretical rate, namely $R=2$ and $R=1$ for the displacement and strains, respectively, which verifies the proof. In Figure 10, the convergence rates in displacement

and energy for FEM and NEM are presented. It is shown that NEM has better absolute accuracy in displacement and strains.

5. Conclusions

Laplace interpolation error estimate is discussed in this study by bounding gradients of the interpolation. It must be noted that, geometric constraints are necessary for guaranteeing the compatibility of polygonal meshes with Laplace interpolation in NEM. The proof of (20) is divided into three parts which are bounded by different constants, and these constants depend on γ^*, d^*, β^* and β_*. Collecting these estimates together gives the final result, i.e., Theorem 2. Some numerical examples are given to show that the computed convergence rate is very close to the theoretical rate.

Although our analysis is based on convex domains, the Laplace interpolation has the ability to exactly impose essential boundary conditions on non-convex domains, which is the significant advantage of the Laplace interpolation, compared to the Sibson interpolation [29].

Acknowledgments

This research was supported by National Natural Science Foundation of China (Nos. 11971386 and 11501450) and China Postdoctoral Science Foundation (No. 2018M633568).

References

[1] Belytschko T, Krongauz Y, Organ D, et al. Meshless methods: An overview and recent developments[J]. Computer Methods in Applied Mechanics and Engineering, 1996, 139(1-4):3-47.
[2] Lucy L B. A numerical approach to the testing of the fission hypothesis[J]. Astronomical Journal, 1977, 82(82):1013-1024.
[3] Gingold R A, Monaghan J J. Smoothed particle hydrodynamics: theory and application to non-spherical stars[J]. Monthly Notices of the Royal Astronomical Society, 1977, 181(3):375-389.
[4] Liu W K, Jun S, Zhang Y F. Reproducing kernel particle methods[J]. International Journal for Numerical Methods in Fluids, 1995, 20(8-9):1081-1106.
[5] Salkauskas P L. Surfaces generated by moving least squares methods[J]. Mathematics of Computation, 1981, 37(155):141-158.
[6] Babuska I, Melenk J M. The partition of unity method[J]. International Journal for Numerical Methods in Engineering, 1997, 40(4):727-758.
[7] Franke R. Scattered data interpolation: tests of some methods[J]. Mathematics of Computation, 1982, 38(157):181-200.
[8] Liu G R, Gu Y T. A point interpolation method for two-dimensional solids[J]. International Journal for Numerical Methods in Engineering, 2001, 50(4):937-951.
[9] Braun J, Sambridge M. A numerical method for solving partial differential equations on highly irregular evolving grids[J]. Nature, 1995, 376(6542):655-660.
[10] Zhang J Y, Emelianenko M, Du Q. Periodic centroidal Voronoi tessellations[J]. International Journal of Numerical Analysis and Modeling, 2012, 9(4):950-969.
[11] Ju L L. Conforming centroidal Voronoi Delaunay triangulation for quality mesh generation[J]. International Journal of Numerical Analysis and Modeling, 2007, 4(3-4):531-547.
[12] Sukumar N, Moran B, Belytschko T. The natural element method in solid mechanics[J]. International Journal for Numerical Methods in Engineering, 1998, 43(5):839-887.
[13] Sukumar N. The natural element method in solid mechanics[M]. Dissertation, Northwestern University, 1998.
[14] Cueto E, Doblare M. The alpha-shapes-based natural element method[C]. Computational Mechanics. 2000.
[15] Cueto E, Doblare M, Gracia L. Imposing essential boundary conditions in the natural element method by means of density-scaled -shapes[J]. International Journal for Numerical Methods in Engineering, 2000, 49(4):519-546.
[16] Bueche D, Sukumar N, Moran B. Dispersive properties of the natural element method[J]. Computational Mechanics, 2000, 25(2-3):207-219.

[17] Toi Y, Kang S S. Mesoscale analysis of solids containing a number of microvoids by using natural element method (1st Report, Evaluation of Overall Elastic Moduli and Yield Stress)[J]. Transactions of the Japan Society of Mechanical Engineers Series A, 2003, 69(683):1101-1107.
[18] Toi Y, Kang S S. Mesoscale analysis of solids containing a number of microvoids by using natural element method (2nd Report, Ductile Fracture Analysis Considering Void Linking)[J]. Transactions of the Japan Society of Mechanical Engineers Series A, 2003, 69(683):1108-1113.
[19] Cai Y, Wang J H. The meshless local-Petrov Galerkin method based on the Voronoi cells[J]. Acta Mechanica Sinica, 2003.
[20] Cai Y, Li X J, Zhu H H. Natural element method based on local Petrov-Galerkin procedure and its object-oriented design and implementation[J]. Chinese Journal of Rock Mechanics & Engineering, 2003, 22(8):1263-1268.
[21] Gonzalez D, Cueto E, Chinesta F, et al. A natural element updated Lagrangian strategy for free-surface fluid dynamics[J]. Journal of Computational Physics, 2007, 223(1):127-150.
[22] Alfaro I, Gagliardi F, Olivera J, et al. Simulation of the extrusion of hollowprofiles by natural element methods[J]. International Journal of Material Forming, 2009, 2(1):597-600.
[23] Cho J R, Lee H W, Yoo W S. Natural element approximation of Reissner-Mindlin plate for locking-free numerical analysis of plate-like thin elastic structures[J]. Computer Methods in Applied Mechanics and Engineering, 2013, 256:17-28.
[24] Lu P, Shu Y, Lu D H, Jiang K Y, et al. Research on Natural Element Method and the application to simulate metal forming processes[J]. Procedia Engineering, 2017, 207:1087-1092.
[25] Bennaceur M A, Xu Y M. Application of the natural element method for the analysis of composite laminated plates[J]. Aerospace Science and Technology, 2019, 87:244-253.
[26] Gillette A, Rand A, Bajaj C. Error estimates for generalized barycentric interpolation[J]. Advances in Computational Mathematics, 2012, 37(3):417-439.
[27] Alexander R, Andrew G, Chandrajit B. Interpolation error estimates for mean value coordinates over convex polygons[J]. Advances in Computational Mathematics, 2013, 39(2):327-347.
[28] Dekel S, Leviatan D. The Bramble–Hilbert lemma for convex domains[J]. SIAM Journal on Mathematical Analysis, 2004, 35(5):1203-1212.
[29] Sukumar N, Moran B, Semenov A Y, et al. Natural neighbour Galerkin methods[J]. International Journal for Numerical Methods in Engineering, 2001, 50(1):1-27.

School of Mathematics and Statistics, Northwestern Polytechnical University, Xi'an, 710072, P. R. China

E-mail: wwzhang@nwpu.edu.cn, 2577901020@mail.nwpu.edu.cn, zzyang@mail.nwpu.edu.cn, yfnie@nwpu.edu.cn